IEEE Access
Multidisciplinary | Rapid Review | Open Access Journal

Received March 31, 2020, accepted April 26, 2020, date of publication May 4, 2020, date of current version May 18, 2020.

Digital Object Identifier 10.1109/ACCESS.2020.2992227

Energy Balancing With Wide Range of Operation in the Isolated Multi-Modular Converter

CRISTIAN VERDUGO[1], (Student Member, IEEE), JOSE IGNACIO CANDELA[1], (Member, IEEE), AND PEDRO RODRIGUEZ[1,2], (Fellow, IEEE)

[1]Electrical Engineering Department, Polytechnic University of Catalonia, 08222 Terrassa, Spain
[2]Science and Technology Institute, Universidad Loyola Andalucía, 41704 Seville, Spain

Corresponding author: Cristian Verdugo (cristian.andres.verdugo@upc.edu)

This work was supported in part by the European Commission under Project FLEXITRANSTORE—H2020-LCE-2016-2017-SGS-774407 and Project INTERRFACE—H2020-LC-SC3-2018-ES-SCC-824330, and in part by the Spanish Ministry of Science under Project ENE2017-88889-C2-1-R.

ABSTRACT The series-connection of modules in multilevel converters are prone to energy imbalances in the dc capacitor due to the differences between the power absorbed and consumed. In renewable energy applications where the primary source is directly connected to each module, energy imbalances can be even worse if the primary sources are affected by unpredictable weather conditions. Therefore, control strategies are required to compensate such energy imbalances, while maintaining the correct converter operation. Focusing our attention on a cascaded transformer multilevel inverter called Isolated Multi-Modular Converter, this paper introduces the combination of two control strategies aimed at providing a wide range of operation under imbalanced energy states. A general analytical model, including the regulation capability and differences with an existing strategy are presented to demonstrate the performance of the control proposed. The effectiveness of the proposal is validated through experimental results based on a three-phase multilevel prototype.

INDEX TERMS Cascaded transformer multilevel inverter, dc energy balancing, isolated multi-modular converter, multilevel converters.

I. INTRODUCTION

Cascaded multilevel converters based on H-bridge (CHB) configurations are among the most suitable multilevel topologies for large-scale photovoltaic (PV) power plants [1]–[4]. The series-connection of modules offers several advantages such as high-quality output voltage, reduced switching frequency and low harmonic distortion, among others. However, the use of multilevel converters for PV applications requires galvanic isolation because most commercial PV modules only tolerate voltage levels between 1000V and 1500V [5]. In order to provide such isolation, extra dc or ac stages are introduced. When galvanic isolation is provided on the dc side, a high-frequency transformer is mandatory in addition to a dc-dc converter. Therefore, maximum power point (MPP) can still be achieved on each PV string connected to the modules. Other multilevel configurations such as Modular Multilevel Converters (MMC) have also been proposed for PV applications [6], all of them based on dc-dc isolated stages.

Conversely, multilevel converters with galvanic isolation through low-frequency transformers have also gained more relevance in literature. Even though, they need bulky transformers, they are highly robust and reliable, important requirements for PV applications. Cascaded transformer multilevel inverters (CTMI) are some of these configurations [7]–[13]. They consist of several H-bridge modules connected in parallel to the same dc source, while the ac side is connected to low-frequency transformers. One of their main advantages is the possibility of setting a certain transformer ratio to reach symmetrical and asymmetrical voltage levels [14]–[16]. However, the limitation of using a single dc source in the case of large power applications has encouraged researchers to find other configurations such as the Isolated Multi-Modular Converter (IMMC) proposed in [17]. The IMMC has two arms in parallel with several modules connected to independent dc sources. Therefore, each PV string is isolated, opening the possibility for high power applications.

The associate editor coordinating the review of this manuscript and approving it for publication was Dragan Jovcic.

The power produced by PV panels is affected by non-uniform irradiance, temperature variations and partial shading. Therefore, if dedicated PV strings are connected to each module, a control strategy is required to operate under imbalanced power circumstances. For cascaded configurations, many control strategies have been proposed to balance the power mismatches between phases and modules of the same phase [18]–[22]. In [20] a control strategy aimed at operating under different power imbalances per phase has been proposed. The control strategy introduces a zero-sequence component in which each voltage reference is compensated according to its respective imbalance ratio. To deal with severe power imbalances, an optimal zero sequence injection is proposed in [21], but this strategy is only suitable for imbalances between phases. In order to control power imbalances between modules of the same phase, a capacitor voltage balancing is proposed in [22]. This strategy phase shifts the modulated voltage according to the dc voltage level. All these strategies have been validated in classical cascaded configurations, but not in the IMMC.

So far, power imbalances in the IMMC have been controlled based on the amplitude voltage compensation [17]. This control strategy was previously proposed for a cascaded H-Bridge multilevel converter in [22], [23] and for a cascaded T-Type configuration in [24]. However, its limited operating range does not allow large power imbalances. This is an important aspect to be considered, since a balance control strategy should have a strong regulatory capacity. Therefore, this paper proposes the combination of two control strategies to provide a wide range of power imbalance. The strategies are based on the amplitude voltage compensation introduced in [17] and on a proposed control strategy called quadrature voltage compensation which phase-shift the modulation index according to the power level of each module.

The rest of the paper is organized as follows: The operation principle of the IMMC and its central control architecture are reviewed in Section II. Then, the concept of power imbalances is described in Section III, where the amplitude and the quadrature voltage compensation are discussed. In section IV the combination of both control strategies are presented to demonstrate their high capability to withstand energy imbalances. Section V presents experimental results based on a three-phase configuration with 2 modules per arm to validate the effectiveness of the presented strategies working individually and combined. Finally, Section VI summarizes the work done.

II. OPERATION PRINCIPLE OF THE IMMC

The three-phase IMMC previously described in [17] is shown in Fig.1. The converter is formed by two arms per phase connected in parallel between a common point n and a coupling inductance L_T, which represents the equivalent inductance of a series-connection of low frequency transformers required to provide galvanic isolation. Each arm has N modules formed by a 2-level voltage source converter and a low frequency transformers, where its primary side is connected to the

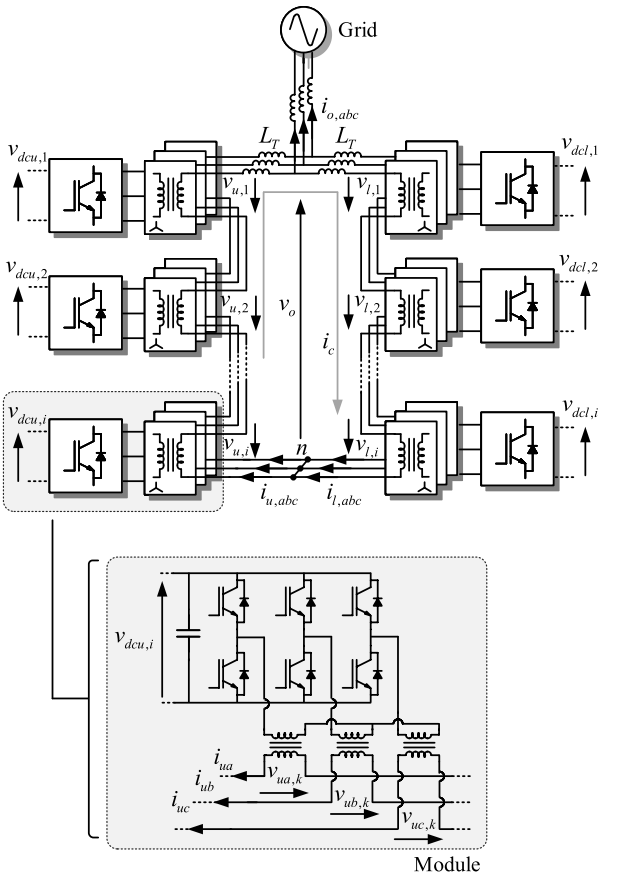

FIGURE 1. Model of the Isolated Multi-Modular Converter.

inverter and the secondary side is connected to the next transformer. Thanks to this galvanic isolation, high floating voltages caused by the series-connection of modules are avoided, making the converter suitable for photovoltaic applications. Additionally, the series connection of modules increases the stepped voltage levels, reducing current harmonics while improving the power quality.

To understand the converter operation, the IMMC can be studied based on the dynamic model of both arms. Referring to each arm as upper and lower arm, from the nomenclature presented in Fig.1, the output and circulating current are given by:

$$i_{o,k} = i_{u,k} - i_{l,k} \tag{1a}$$

$$i_{c,k} = \frac{i_{u,k} + i_{l,k}}{2} \tag{1b}$$

The subscript u and l represent the upper and lower arm in phase k, $i_{o,k}$ is the output current and $i_{c,k}$ is the circulating current flowing through the converter when there is an imbalanced energy operation.

Considering the fact that each module generates an output voltage $v_{x,k,i}$ in the secondary side of the transformer, where x is the upper or lower arm and i represents the module, the voltage arm given by the series-connection of modules

per phase is reduced to:

$$v_{x,k} = \sum_{i=1}^{N} v_{x,k,i} \tag{2}$$

Introducing the Kirchhoff's voltage law in combination with the current and voltage expressions defined in (1) and (2), the dynamic model per phase of the IMMC is given by:

$$\frac{R_T}{2} i_{o,k} + \frac{L_T}{2} \frac{d}{dt} i_{o,k} = v_{s,k} - v_{o,k} \tag{3a}$$

$$R_T i_{c,k} + L_T \frac{d}{dt} i_{c,k} = v_{c,k} \tag{3b}$$

where L_T is the equivalent winding inductance defined by the low frequency transformers and R_T is the equivalent resistance used to model the arm losses. Note that two decoupled dynamic models have been declared to represent the output and circulating current behavior. In the case of the output current model, voltage $v_{s,k}$ represents the voltage difference between the upper and lower arms. Similarly, in the circulating current model, voltage $v_{c,k}$ is the average voltage arm, which also represents the voltage drop in the coupling inductance. These voltages can be described in terms of the voltage arms as follows:

$$v_{s,k} = \frac{v_{l,k} - v_{u,k}}{2} \tag{4a}$$

$$v_{c,k} = \frac{v_{u,k} + v_{l,k}}{2} \tag{4b}$$

These models can also be expressed in terms of the *dq* reference frame. Consequently, applying the Park transformation to equation (3), the dynamic models are expressed according to equations (5) and (6).

$$\frac{R_T}{2} i_{od} + \frac{L_T}{2} \frac{d}{dt} i_{od} - j\omega i_{oq} = v_{sd} - v_{od} \tag{5a}$$

$$\frac{R_T}{2} i_{oq} + \frac{L_T}{2} \frac{d}{dt} i_{oq} + j\omega i_{od} = v_{sq} - v_{oq} \tag{5b}$$

$$R_T i_{cd} + L_T \frac{d}{dt} i_{cd} - j\omega i_{cq} = v_{cd} \tag{6a}$$

$$R_T i_{cq} + L_T \frac{d}{dt} i_{cq} + j\omega i_{cd} = v_{cq} \tag{6b}$$

A. INSTANTANEOUS POWER ANALYSIS

The energy operation of each module is closely related to the power flow between the primary source connected to the dc side and the active power delivered into the grid. Any power mismatch caused by a variation in the dc or ac side will create an energy imbalance which has to be compensated to allow a stable operation.

The energy analysis is carried out considering an average model per arm where the series-connection of modules is evaluated based on the ac voltage and current signals. Therefore, the active power in both arms are given by:

$$\begin{aligned} p_{ou} &= \frac{3}{2}\Re\left[\left(v_{ud} + jv_{uq}\right)\left(i_{ud} - ji_{uq}\right)\right] \\ &= \frac{3}{2}\Re\left[\left(v_{ud} + jv_{uq}\right)\left(\frac{i_{od} - ji_{oq}}{2} + i_{cd} - ji_{cq}\right)\right] \\ &= \frac{3}{2} v_{ud}\left(\frac{i_{od}}{2} + i_{cd}\right) + \frac{3}{2} v_{uq}\left(\frac{i_{oq}}{2} + i_{cq}\right) \end{aligned} \tag{7}$$

$$\begin{aligned} p_{ol} &= \frac{3}{2}\Re\left[\left(v_{ld} + jv_{lq}\right)\left(i_{ld} - ji_{lq}\right)\right] \\ &= \frac{3}{2}\Re\left[\left(v_{ld} + jv_{lq}\right)\left(-\frac{i_{od} - ji_{oq}}{2} + i_{cd} - ji_{cq}\right)\right] \\ &= \frac{3}{2} v_{ld}\left(-\frac{i_{od}}{2} + i_{cd}\right) + \frac{3}{2} v_{lq}\left(-\frac{i_{oq}}{2} + i_{cq}\right) \end{aligned} \tag{8}$$

To observe the impact of the output and circulating currents on the active power, the current arms have been replaced according to equation (1) and decomposed into their *dq* components. A dependency of the output and circulating currents in both arms can be appreciated. This can also be seen when the total and the difference active powers are defined.

$$p_T = \frac{3}{2}(v_{sd} i_{od} + 2v_{cd} i_{cd}) + \frac{3}{2}\left(-v_{sq} i_{oq} + 2v_{cq} i_{cq}\right) \tag{9}$$

$$p_\Delta = \frac{3}{2}\left(v_{cd} i_{od} - 2v_{sd} i_{cd}\right) + \frac{3}{2}\left(v_{cq} i_{oq} - v_{sq} i_{cq}\right) \tag{10}$$

According to (9) and (10), the total and the difference active powers represent the power delivered into the grid and the power imbalance between the upper and lower arms. Note how the *d* components of the output and circulating currents are associated to v_{sd} and v_{cd}, while the *q* current components are related to the voltages v_{sq} and v_{cq}.

It is assumed that the equivalent coupling inductances are quite small and, consequently, their voltage drops can be neglected. Therefore, the voltage arms are reduced to $v_{udq} = -v_{odq}$ and $v_{ldq} = v_{odq}$. Under this assumption, the total power is given by:

$$p_T = -\frac{3}{2}\left(v_{od} i_{od} + v_{oq} i_{oq}\right) \tag{11}$$

Similarly, the power difference yields:

$$p_\Delta = -3\left(v_{od} i_{cd} + v_{oq} i_{cq}\right) \tag{12}$$

The definition of both active power components helps defining the dependency between the voltage and current signals required to set the appropriate references for the central control architecture of the IMMC.

B. CENTRAL CONTROL DESCRIPTION

As discussed in previous section, the total and the difference active powers are used to define the current references according to the total energy in the series-connection of modules. The relationship between the active power and the energy variation is given by the rate of energy change in the dc capacitor. According to [17], the rate of change is defined as:

$$P_{o,x} = \frac{C_{sm}}{2N} \frac{d}{dt}\left(v_{dc,i}^{\Sigma}\right)^2 \tag{13}$$

where N is the number of modules per arm, C_{sm} is the dc capacitance and $v_{dc,i}^{\Sigma}$ is the addition of all dc voltages per arm.

The dynamic model of the current arms and the rate of energy change in the dc capacitors can be used to define the control architecture oriented to regulate the average operation

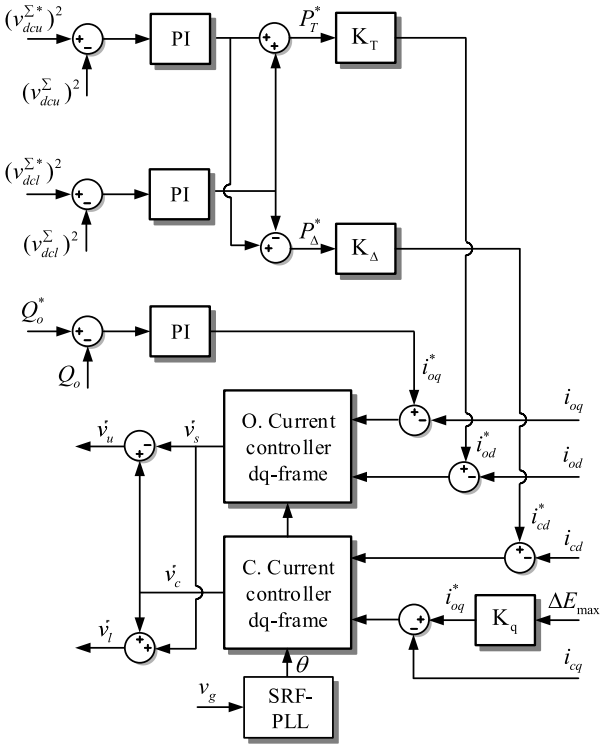

FIGURE 2. Central control architecture.

of the converter. The control architecture used in the IMMC includes two control loops as described below:

- The internal output and circulating current control loops based on PI controllers are required to provide a perfect tracking and avoid overcurrent levels.
- The external dc voltage control loops are required to define the output and circulating current references based on the total dc voltage and the rate of energy change provided by the series-connection of all modules per arm.

The control architecture shown in Fig.2 has two external control loops to process the error between the reference and the measured dc voltages. Afterwards, the total and the difference active powers are multiplied by variables K_T and K_Δ inferred from equations (11) and (12) to transform the power signals into the output and the circulating current references. A Phase-Locked-Loop (PLL) synchronizes the current signals with the ac grid forcing the q component of the ac voltage to zero. This generates a direct correlation between the active power and the d components of the current references. Likewise, the reactive power is related to the q component of the output current reference.

The central control architecture defines the signals $\vec{v}_s$ and $\vec{v}_c$ which according to (14) represent the dq components of v_s and v_c respectively. Then, a decoupling stage based on (4) is used to obtain the average modulated voltages $\vec{v}_u$ and $\vec{v}_l$. Note that these signals do not differentiate between modules with higher or lower energy levels. This may result in instability issues, causing converter failures when the modules operate under energy imbalances. In order to solve this problem, a local control strategy has to be included to regulate the modulation index in accordance to the power and dc voltage levels.

$$\vec{v}_s = \begin{bmatrix} v_{sd} \\ v_{sq} \end{bmatrix}, \quad \vec{v}_c = \begin{bmatrix} v_{cd} \\ v_{cq} \end{bmatrix}, \quad \vec{v}_x = \begin{bmatrix} v_{xd} \\ v_{xq} \end{bmatrix} \tag{14}$$

III. AMPLITUDE AND QUADRATURE VOLTAGE COMPENSATION

The series-connection of modules sets out several challenges to balance the energy and provides a stable state. Since each module is connected to independent dc sources, the probability of having different dc voltage levels is not low. Therefore, a control strategy to locally adapt the modulation index according to the dc voltage, allowing a certain range of energy imbalance is necessary.

So far, the central control architecture defines the average modulation index in all modules of the upper and lower arms. However, this control layer does not differentiate between modules with higher or lower energy levels, triggering to instabilities when modules generate difference power levels. As described in previous work [17], the energy balance is defined by the power exchange between the dc and ac side of one module, giving rise to:

$$P_{cx,i} = P_{dcx,i} - P_{ox,i} \tag{15}$$

where $P_{cx,i}$, is the absorbed or delivered power from the dc capacitor, $P_{dcx,i}$ is the dc power provided by the external source and $P_{ox,i}$ is the output power delivered into the grid. Note that the power from the dc capacitor is governed by the power difference between the external source and the ac grid, generating a positive value when $P_{ox,i} < P_{dcx,i}$ and a negative value when $P_{ox,i} > P_{dcx,i}$. Depending on the power sign, the dc voltage will increase or decrease due to the power expression described in (16).

$$P_{cx,i} = \frac{C_{sm}}{2} \frac{d}{dt} \left(v_{dcx,i}^2 \right) \tag{16}$$

The rate of energy change in the capacitor will increase the dc voltage when the power is positive and reduce it when the power is negative. Since the amount of energy is directly proportional to the quadratic dc voltage, a higher voltage level in the capacitor holds a higher energy. On the other hand, a lower dc voltage means a lower energy level. In order to regulate the amount of energy, it is necessary to control the power flow between the external source and the output power, so the dc voltage is set to a certain level. However, the dc source is affected by external conditions, which implies a higher uncertainty in its power production. Consequently, the energy balance can be regulated by using the output power, while the external dc source is considered as a perturbation. The output power in each module is given by:

$$P_{ox,i} = v_{x,i} i_x \cos(\theta_{x,i}) \tag{17}$$

Equation (17) shows that the output power is affected by three different variables: the magnitude of the ac voltage,

the magnitude of the current arm and the phase angle between both signals. Owing to the current arm is a common variable in the series-connection of modules, the ac voltage and the phase angle are the only variables in each module capable of controlling the power flow individually. Therefore, the energy balance can be achieved by a local controller which adjusts the average modulation index considering either the amplitude ac voltage or its phase angle.

Based on this concept, the amplitude and quadrature voltage compensation strategies are described to withstand the energy imbalances.

A. CONTROL STRATEGY BASED ON AMPLITUDE VOLTAGE COMPENSATION

The amplitude voltage compensation has been previously described in [22]– [24]. This well-known control strategy modifies the modulated ac voltage $v_{x,i}$ amplitude in each module to adjust the active power flow and control the energy in the dc capacitor. To understand how the control strategy works, a vector analysis is presented in Fig.3. Vectors $v_{x,1}$, $v_{x,2}$, and $v_{x,3}$ represent the voltage state of three modules before adding the amplitude voltage compensation. By adding them up with the drop voltage of the coupling inductance, the output voltage v_o is defined. Note that the current arm i_x is shifted θ_i degrees in relation to the output voltage. This phase shift defines the direction of the drop voltage in L_T.

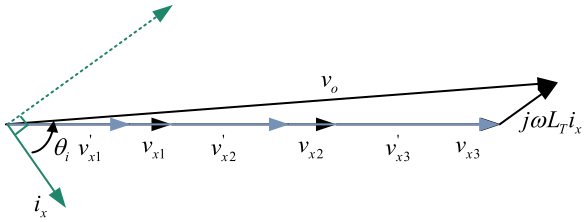

FIGURE 3. Vector analysis of control strategy based on amplitude voltage compensation.

After adding the amplitude voltage compensation, voltages $v_{x,1}$, $v_{x,2}$, and $v_{x,3}$ become $v'_{x,1}$, $v'_{x,2}$, and $v'_{x,3}$, respectively. Voltages v'_{x1} and v'_{x2} reduce their magnitude to reduce their output power, while v'_{x3} increases its magnitude to increase its output power, ensuring a complete balance operation. Since the amplitude voltage is linked to the d component of the modulation index, the amplitude voltage compensation acts directly in the voltage arm v_{xd} given by the central control. Therefore, according to the control architecture of Fig.2, the local modulation index of each module after adding the voltage compensation yields:

$$\frac{2N}{v^{\Sigma}_{dc,x}} v_{xd} + k_x \Delta m_{xd,i} = m^*_{xd,i} \tag{18}$$

where $2N/v^{\Sigma}_{dc,x}$ is the constant required to normalize the control signal v_{xd} between -1 and 1, $\Delta m_{xd,i}$ is the compensation provided by the amplitude voltage control and $m^*_{xd,i}$ is the new modulation index required to achieve the local voltage reference. The control architecture of the amplitude voltage compensation is illustrated in Fig.4.

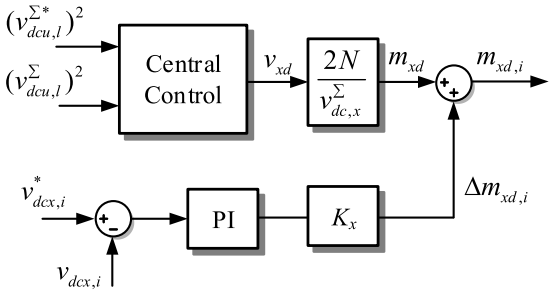

FIGURE 4. Control architecture of the amplitude voltage compensation.

The error between the voltage reference given by a maximum power point tracking (MPPT) algorithm or any other reference and the voltage measurement is processed through a PI controller. This defines the compensation value required to increase or decrease the amplitude of the average modulation index. Depending on whether the module belongs to the upper or lower arms, the compensation signal is added or subtracted from the average modulation index through the constant k_x.

B. CONTROL STRATEGY BASED ON QUADRATURE VOLTAGE COMPENSATION

As previously stated, the output power of each module is commanded by the amplitude of the modulated voltage and its phase angle. In this second control strategy, the phase angle is used to phase shift the output voltage and regulates the energy level in the dc capacitor.

According to equations (7) and (8), the power arm is defined by the product between the current and voltage arms. Therefore, the output power per module in the dq reference frame can be reduced to:

$$p_{ox,i} = \frac{3}{2}\left(v_{xd,i} i_{xd} + v_{xq,i} i_{xq}\right) \tag{19}$$

Voltage v_{xd} is associated to the voltage amplitude used to control the power flow in previous control strategy. On this occasion, voltage v_{xq} causes the power regulation. However, this voltage will not have any effect on the energy regulation if the q component of the current arm is zero. Since the current arm depends on the output and circulating currents, when no reactive power is produced, the output current i_{oq} is zero. This creates a dependency on the q component of the circulating current to control the power. As seen in the previous section, the central control architecture contains a droop gain K_q for setting the circulating current reference i^*_{cq}. Thus, the circulating current reference is given by:

$$i^*_{cq} = \Delta E_{\max} \cdot K_q \tag{20}$$

Energy ΔE_{max} defines the maximum energy difference between the series-connection of modules in one arm, while

the droop gain K_q is defined according to the maximum circulating current allowed in the converter. A higher i_{cq} generates a larger phase shift in the current arm. However, the limitation of this current component is defined by the maximum current allowed in the converter, which will contribute to adjust the phase angle as:

$$\theta_i' = \tan^{-1}\left(\frac{i_{xq}}{i_{xd}}\right) \tag{21}$$

After the circulating current i_{cq} is defined, it is necessary to generate the proper output voltage $v_{xq,i}$ to control the power flow of each module. The vector analysis shown in Fig.5 describes the operation principle of the control strategy based on the phase angle, also known as quadrature voltage compensation.

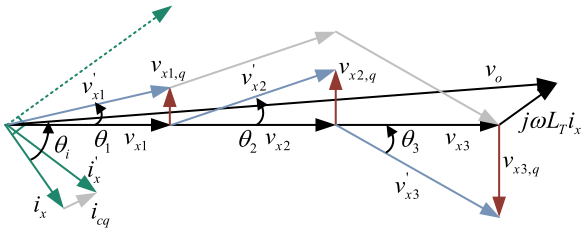

FIGURE 5. Vector analysis of control strategy based on quadrature voltage compensation.

Before adding the quadrature voltage compensation, voltages v_{x1}, v_{x2} and v_{x3} represent the output voltage of three modules. By adding them up plus the drop voltage in the coupling inductance, the voltage v_o modulated in the ac terminals is defined. Nevertheless, after adding the quadrature voltage compensation, the q component of $v_{x,i}$ modifies the phase angle of each module while the circulating current i_{cq} modifies θ_i. Therefore, the output voltages become v_{x1}', v_{x2}' and v_{x3}', while the local phase angles change to θ_1, θ_2 and θ_3. The addition of θ_1 and θ_2 to the phase angle θ_i' reduces the power provided by modules 1 and 2, while the phase angle θ_3 increases the power provided by module 3.

Similar to the analysis described in the amplitude voltage compensation, the modulation index given by the q component of the voltage arm in the central controller after adding the quadrature voltage compensation is reduced to.

$$\frac{2N}{v_{dcx}^{\Sigma}} v_{xq} + \Delta m_{xq,i} = m_{xq,i}^{*} \tag{22}$$

Variable v_{xq} is the q voltage component brought about the central controller, $\Delta m_{xq,i}$ is the compensation required to adjust the dc voltage level and $m_{xq,i}^{*}$ is the new modulation index in module i. The control architecture of the quadrature voltage compensation is shown in Fig.6.

The voltage difference between the reference and the measurement signal is processed through a PI controller which sets the compensation of the average modulation index. Note that the circulating current sign is required to add or subtract the compensation from m_{xq}.

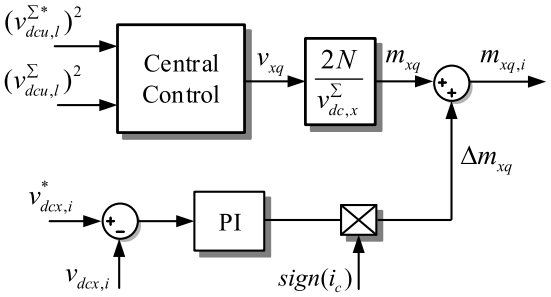

FIGURE 6. Control architecture of the quadrature voltage compensation.

IV. COMBINATION OF BOTH CONTROL STRATEGIES

The overmodulation defines the maximum operating range to withstand energy imbalances. Therefore, If the converter run close to the overmodulation level, the capability to tolerate imbalances will be small. This is one of the main drawbacks in the amplitude voltage compensation as it has a direct effect on the modulation index amplitude. On the other hand, the quadrature voltage compensation phase shifts the modulated voltage based on the circulating current i_{cq}. As a result, high levels of circulating currents may increase the capability to tolerate high energy imbalances but also the converter losses.

The combination of both control strategies can be used to withstand high levels of energy imbalances, reducing the circulating current by adjusting at the same time the amplitude and the phase angle of the modulated signals. In order to analyze the operating range of both control strategies, in Fig.7 is shown the modulation index response of one module operating under multiple power deviations. The analysis starts with three modules per arm producing the same power level. Then, the first module decreases its power to increase the power imbalance. Fig.7.a shows the modulation response of the IMMC based on the amplitude and quadrature voltage compensation working individually. In the case of the amplitude voltage compensation, a small power deviation triggers to a fast increase in the modulation index. The maximum power deviation achieved before overmodulation is 40%.

Using the quadrature voltage compensation, the capability to tolerate energy imbalances is higher than the amplitude voltage compensation. When the circulating current i_{cq} is 25% the nominal current arm, the modulation index reaches the overmodulation at 45% of power. Nevertheless, as the circulating current increases, the control strategy is able to withstand larger energy imbalances. Note that a circulating current of 45% is capable to tolerate a power deviation of 75%.

However, implementing the amplitude and the quadrature voltage compensation together, the capability to withstand energy imbalances is even higher. Fig.7.b shows how a circulating current of 25% tolerates a 70% of power imbalance and a 100% of power imbalance with a circulating current of 45%.

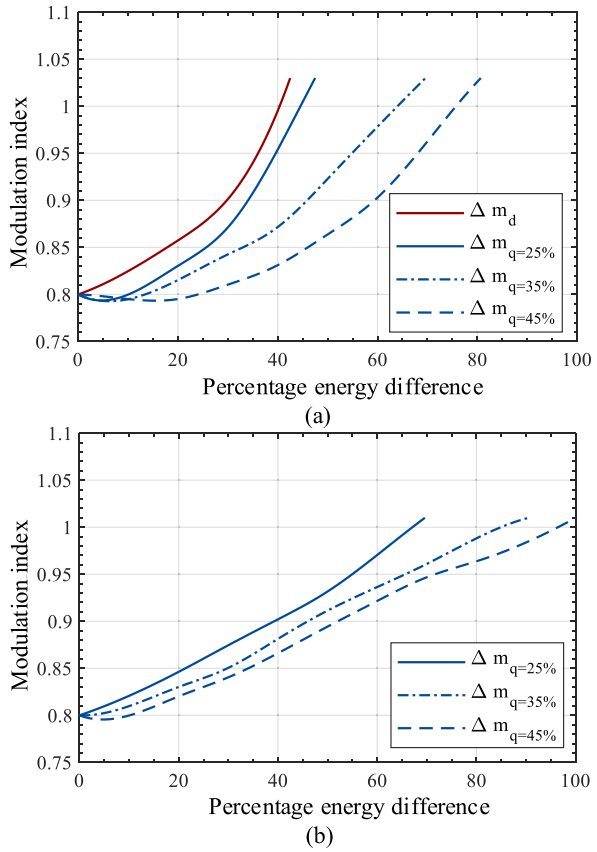

FIGURE 7. Modulation index response under several power changes. (a) Amplitude and Quadrature voltage compensation working individually, (b) Combination of both control strategies.

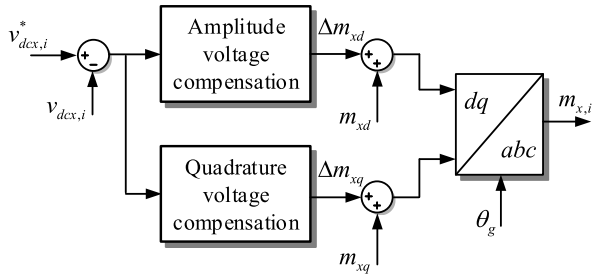

FIGURE 8. Control diagram based on the combination of both control strategies.

The control architecture embedded in each module based on both control strategies is illustrated in Fig.8. The error between the voltage reference and the voltage measured is processed through both control loops. The amplitude voltage compensation regulates the d component of the modulation index, while the quadrature voltage compensation regulates the q component.

V. EXPERIMENTAL RESULTS

In an attempt to clarify and validate the IMMC working under energy imbalances, a 4.8 kW prototype with two modules per arm is tested with both control strategies. In the first scenario, the amplitude and quadrature voltage compensation are individually evaluated, then the combination of both strategies are used to show the higher tolerance under energy imbalances. The laboratory setup and its electrical circuit diagram are shown in Fig.9. Two modules based on three-phase inverters are connected in series through the secondary winding of three-phase transformers. Additionally, an LC filter is used to mitigate high frequency components, reducing the ac current ripple. On the other hand, to emulate four independent PV panels, a programmable dc source (Magna-Power TSD1000-20/36) is connected in series to dc resistors, emulating the voltage range between the maximum power and open-circuit operation. The central and local controllers are implemented in control platforms based on DSPs TMS320F28335 from Texas Instrument. In the central control platform, the average dc voltage and the internal current control loops are evaluated. The local control platforms embedded in each converter cabinet are used to balance the energy, set physical signals and provide voltage and current protections. The status variables and control signals are transmitted through a bidirectional communication bus based on a CAN-open protocol.

TABLE 1. Experimental parameters.

Parameters	Symbol	Value
Nominal Power	P_o	4.8kW
Nominal Power per module	$P_{x,i}$	1.2kW
Grid Voltage	v_g	320V
Grid Frequency	f_g	50Hz
Number of modules per arm	N	2
dc-link Capacitance	C_{sm}	4700μF
dc Resistor	$R_{dc,i}$	22.5Ω
Switching Frequency	f_s	8200 Hz
Open-circuit voltage	v_{op}	440V
MPP Voltage	v_{mp}	360V
Inductance LC Filter	L_f	3mH
Capacitance LC Filter	C_f	5μF
Transformer Voltage	V_T	400V
Transformer Power	P_T	2kW
Transformer inductance	L_{T1}	8.3mH

The connection between the IMMC converter and the ac grid is performed through an auto-transformer to operate at 320 V_{LLRMS}/ 50 Hz. All parameters are listed in Table 1.

In order to evaluate the maximum energy difference, dc voltage steps are set in the upper and lower arm modules. The voltage, current and power response are illustrated from Fig.10 to Fig.14.

A. IMBALANCE ENERGY OPERATION BASED ON AMPLITUDE AND QUADRATURE VOLTAGE COMPENSATION

In the first study case, the imbalance energy operation is evaluated using individually the amplitude and quadrature voltage

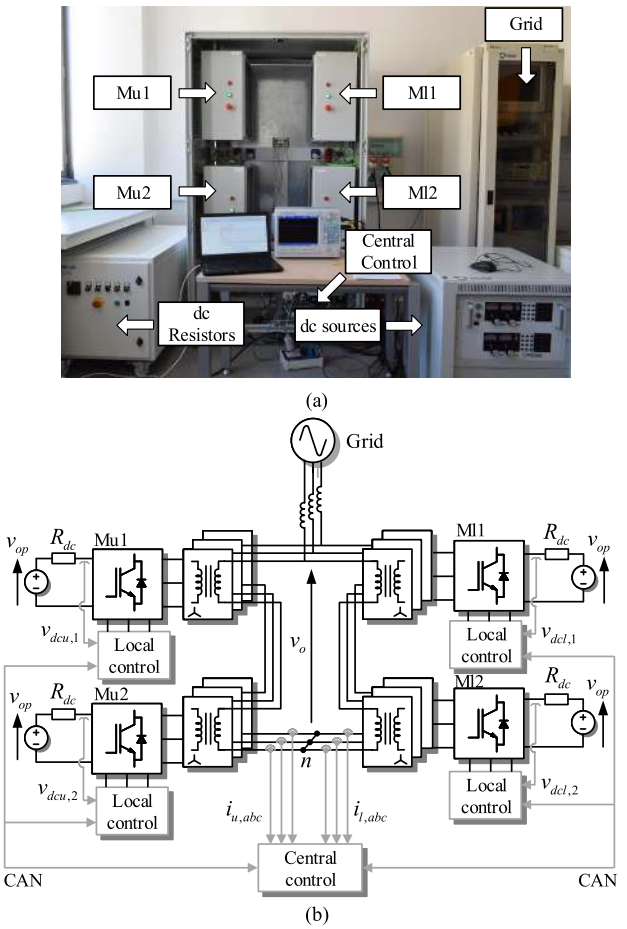

FIGURE 9. Experimental setup. (a) Laboratory setup, (b) Electrical circuit diagram.

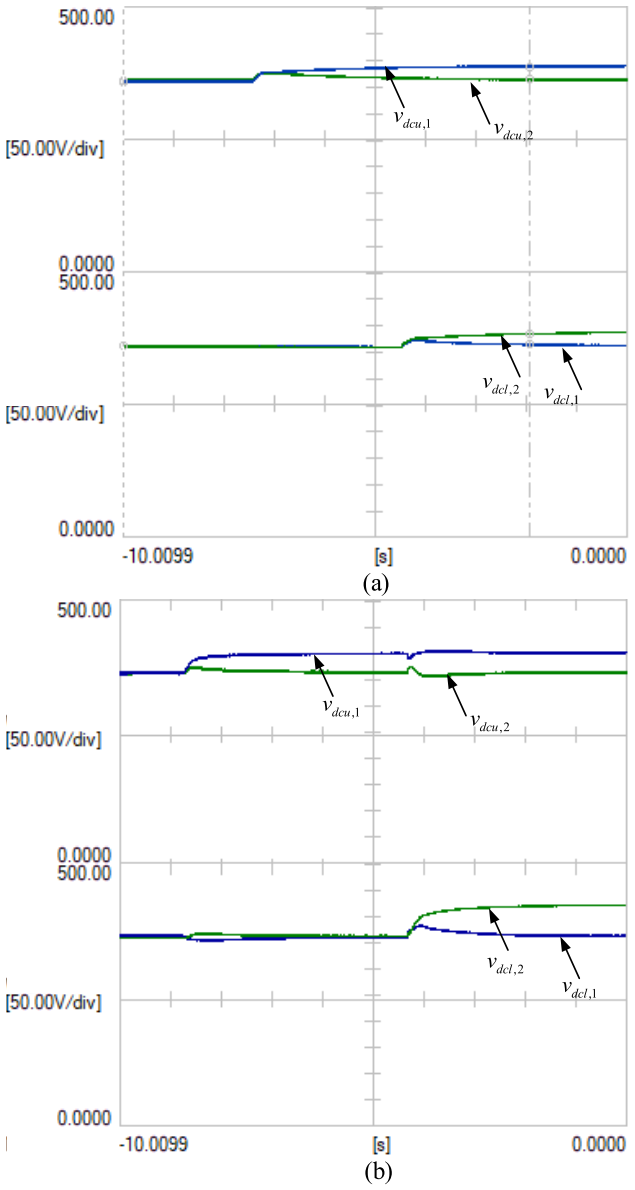

FIGURE 10. Steady and dynamic state response of dc voltages in the upper and lower arms with a control strategy based on: (a) Amplitude voltage compensation,(b) Quadrature voltage compensation.

compensation. In Fig.10.a, a dc voltage step is introduced in module M_{u1} to operate the upper arm at different energy levels based on the amplitude voltage compensation. This change is conducted by increasing the dc voltage from 360V to 390V, giving rise to a power decrease of 390W. The new power level creates a power difference between the upper and lower arm, triggering to a circulating current flowing through the converter. Due to the fact that the amplitude voltage compensation set the q component of the circulating current to 0, the difference between the upper and lower power arms is directly related to the current amplitude.

In Fig.11.a, the phase a of the current arms are illustrated before and after the voltage step is set in module M_{u1}. Owing to all modules operate at maximum power (1.2 kW), the current arms have the same amplitude but shifted 180°. However, after the dc voltage of module M_{u1} increases to 390V, the upper current arm decreases as the circulating current increases. Remember that the amplitude voltage compensation has a direct effect on the modulation index amplitude, therefore, its control range is restricted by the overmodulation level.

After 3s, a second voltage step is introduced in the second module M_{l2} of the lower arm. Fig.10.a illustrates how the dc voltage $v_{dcl,2}$ increases from 360V to 390V, triggering to a power decrease of 390W. This second power step creates an energy imbalance between the modules, but since both arms generate the same power, no circulating current flows through the converter.

A similar scenario is conducted using the quadrature voltage compensation. However, due to the higher capability to tolerate energy imbalances, on this occasion a dc voltage step of 40V is introduced in the upper arm module M_{u1} and a second voltage step of 60V is introduced in the lower arm module M_{l2}, as seen in Fig.10.b. To withstand these energy imbalances, a circulating current i_{cq} of 35% the nominal current arm has been set. In Fig.11.b is illustrated how this circulating current component phase shifts the current arm after

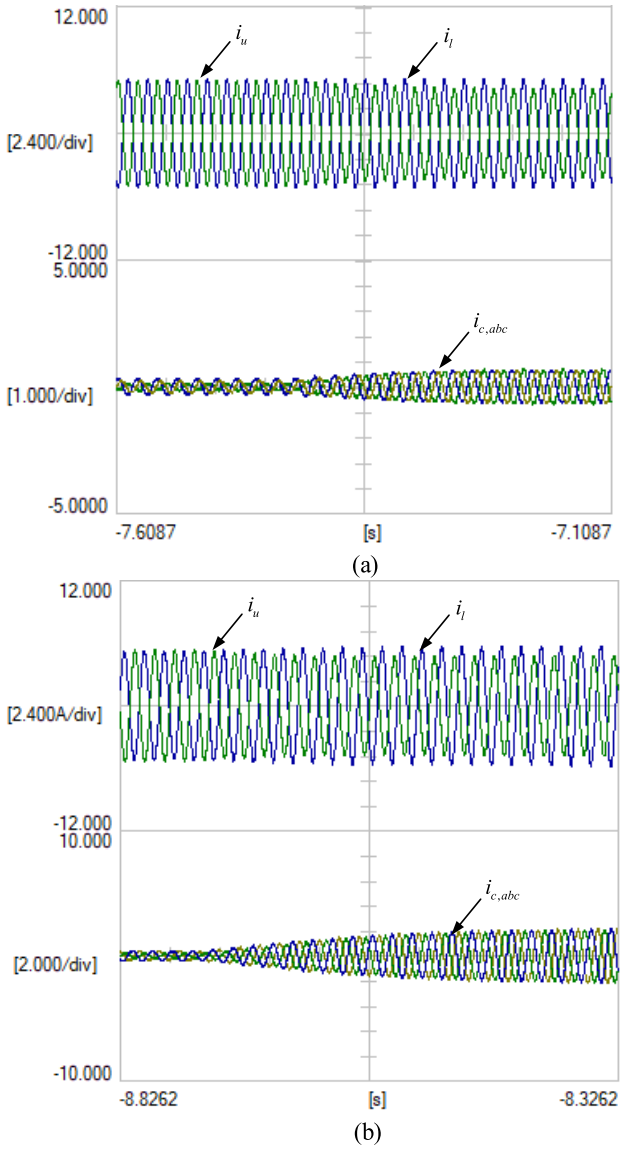

FIGURE 11. Current arms and circulating current of the IMMC based on: (a) Amplitude voltage compensation, (b) Quadrature voltage compensation.

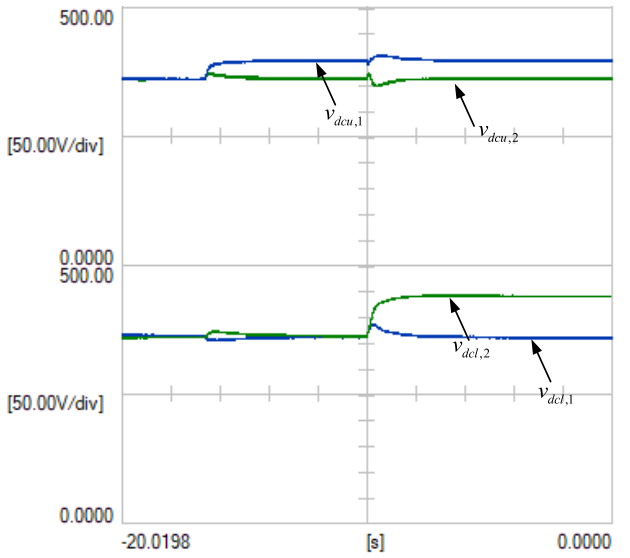

FIGURE 12. Steady and dynamic state response of dc voltages in the upper and lower arms using the combination of the amplitude and quadrature voltage compensation.

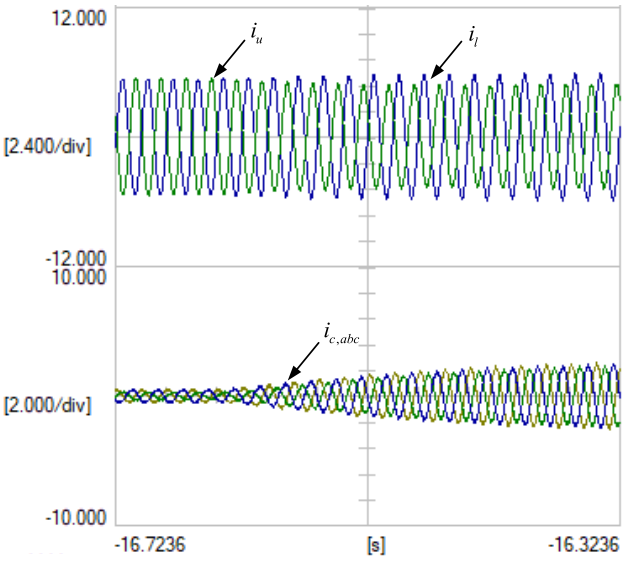

FIGURE 13. Current arms and circulating current using the combination of the amplitude and quadrature voltage compensation.

the dc voltage in M_{u1} increases. Additionally, it is observed a reduction in the amplitude of the upper current arm due to the power decrease.

B. IMBALANCED ENERGY OPERATION BASED ON THE COMBINATION OF THE AMPLITUDE AND QUADRATURE VOLTAGE COMPENSATION

In previous study case, the amplitude and quadrature voltage compensation where individually evaluated, demonstrating that the quadrature voltage compensation provides a higher capability to tolerate energy imbalances. In this study case, the combination of both strategies are evaluated to increase even more the energy imbalance operation. Similar to the previous case, two dc voltage steps are introduced. However, the capability to handle larger energy imbalances allows bigger voltage steps. The results are described in Fig.12 and Fig.13.

Before the voltage steps, all modules operate at nominal power. After 3.5s, a voltage step of 40V is introduced in M_{u1}, increasing the dc voltage from 360V to 400V. Since both control strategies are used, a circulating current i_{cq} equal to 35% the nominal current arm is set to withstand this energy imbalance. Fig.13 shows how the upper and lower current arms are phase shifted as the circulating current increases. Note that an intrinsic circulating current i_{cd} arises, as a consequence of the current difference between the upper and lower arms.

Combining both control strategies, the voltage compensation adjusts the d and q components of the control signals at

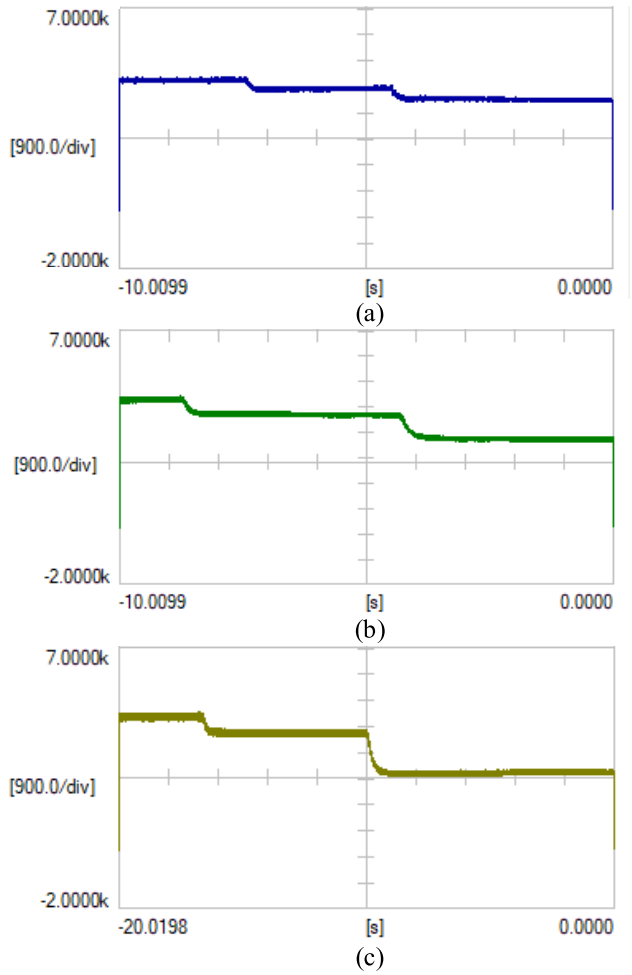

FIGURE 14. Output power based on, (a) Amplitude voltage compensation, (b) Quadrature voltage compensation, (c) Combination of both control strategies.

the same time. In order to evaluate the higher capability to withstand energy imbalances, a second voltage step of 80V is introduced in M_{l2}. This voltage creates a large power decrease in M_{l2}. However, it can be seen how the converter is able to withstand such energy imbalance.

C. COMPARATIVE ANALYSIS BETWEEN BOTH CONTROL STRATEGIES

The power response of all previous scenarios are studied in Fig.14. The energy imbalance based on the amplitude voltage compensation allows a maximum power difference of 33% between the two modules connected in series. However, in the quadrature voltage compensation, the circulating current i_{cq} introduced allows a power difference of 65% as seen in the second power step of Fig.14.b. When combining both control strategies the operating range become significantly larger, allowing higher energy imbalances. In Fig.14.c is illustrated how the second voltage step decreases the power generated by module M_{l2} close to zero, creating a power difference of 100%.

VI. CONCLUSION

This paper has proposed the combination of two control strategies in the Isolated Multi-Modular Converter to withstand wide energy imbalances in the series connection of modules. The control strategies are embedded in each module and adjust the average modulation index provided by the central controller, which regulates the total energy per arm through two current control loops. The control strategy proposed regulates the amplitude and phase angle of the modulation index. The amplitude voltage compensation adjusts the d component of the modulation index, while the quadrature voltage compensation adjusts the phase angle through the q voltage component. Experimental results based on two modules per arm have validated the effectiveness and feasibility of the control proposed, demonstrating that the IMMC is able to withstand large levels of energy imbalances and operates even if some modules decrease their power to critical levels.

REFERENCES

[1] W. Zhao, H. Choi, G. Konstantinou, M. Ciobotaru, and V. G. Agelidis, "Cascaded H-bridge multilevel converter for large-scale PV grid-integration with isolated DC-DC stage," in *Proc. 3rd IEEE Int. Symp. Power Electron. Distrib. Gener. Syst. (PEDG)*, Aalborg, Denmark, Jun. 2012, pp. 849–856.

[2] S. Busquets-Monge, J. Rocabert, P. Rodriguez, S. Alepuz, and J. Bordonau, "Multilevel diode-clamped converter for photovoltaic generators with independent voltage control of each solar array," *IEEE Trans. Ind. Electron.*, vol. 55, no. 7, pp. 2713–2723, Jul. 2008.

[3] S. Essakiappan, H. S. Krishnamoorthy, P. Enjeti, R. S. Balog, and S. Ahmed, "Multilevel medium-frequency link inverter for utility scale photovoltaic integration," *IEEE Trans. Power Electron.*, vol. 30, no. 7, pp. 3674–3684, Jul. 2015.

[4] C. D. Fuentes, C. A. Rojas, H. Renaudineau, S. Kouro, M. A. Perez, and T. Meynard, "Experimental validation of a single DC bus cascaded H-Bridge multilevel inverter for multistring photovoltaic systems," *IEEE Trans. Ind. Electron.*, vol. 64, no. 2, pp. 930–934, Feb. 2017.

[5] E. Serban, M. Ordonez, and C. Pondiche, "DC-bus voltage range extension in 1500 v photovoltaic inverters," *IEEE J. Emerg. Sel. Topics Power Electron.*, vol. 3, no. 4, pp. 901–917, Dec. 2015.

[6] M. A. Perez, D. Arancibia, S. Kouro, and J. Rodriguez, "Modular multilevel converter with integrated storage for solar photovoltaic applications," in *Proc. 39th Annu. Conf. IEEE Ind. Electron. Soc. (IECON)*, Vienna, Austria, Nov. 2013, pp. 6993–6998.

[7] J. P. R. A. Mello, C. B. Jacobina, and A. P. Monteiro, "Multilevel single-phase PWM converters with shared legs and cascaded transformers," in *Proc. IEEE Energy Convers. Congr. Exposit. (ECCE)*, Baltimore, MD, USA, Sep. 2019, pp. 5878–5885.

[8] A. K. Panda and Y. Suresh, "Performance of cascaded multilevel inverter by employing single and three-phase transformers," *IET Power Electron.*, vol. 5, no. 9, pp. 1694–1705, Nov. 2012.

[9] A. A. Gandomi, S. Saeidabadi, S. H. Hosseini, E. Babaei, and Y. A. Gandomi, "Flexible transformer-based multilevel inverter topologies," *IET Power Electron.*, vol. 12, no. 3, pp. 578–587, Mar. 2019.

[10] S. Salehahari, E. Babaei, S. H. Hosseini, and A. Ajami, "Transformer-based multilevel inverters: Analysis, design and implementation," *IET Power Electron.*, vol. 12, no. 1, pp. 1–10, Jan. 2019.

[11] S. Behara, N. Sandeep, and U. R. Yaragatti, "Design and implementation of transformer-based multilevel inverter topology with reduced components," *IEEE Trans. Ind. Appl.*, vol. 54, no. 5, pp. 4632–4639, Sep. 2018.

[12] H. K. Jahan, K. Zare, and M. Absapour, "Verification of a low component nine-level cascaded-transformer multilevel inverter in grid-tied mode," *IEEE J. Emerg. Sel. Topics Power Electron.*, vol. 6, no. 1, pp. 429–440, Mar. 2018.

[13] N. N. V. S. Babu and B. G. Fernandes, "Cascaded two-level inverter-based multilevel STATCOM for high-power applications," *IEEE Trans. Power Del.*, vol. 29, no. 3, pp. 993–1001, Jun. 2014.

[14] F. A. D. C. Bahia, C. B. Jacobina, N. Rocha, and R. P. R. de Sousa, "Cascaded transformer multilevel inverters with asymmetrical turns ratios based on NPC," *IEEE Trans. Ind. Electron.*, vol. 67, no. 8, pp. 6387–6397, Aug. 2020.
[15] O. Lopez-Santos, C. A. Jacanamejoy-Jamioy, D. F. Salazar-D'Antonio, J. R. Corredor-Ramirez, G. Garcia, and L. Martinez-Salamero, "A single-phase transformer-based cascaded asymmetric multilevel inverter with balanced power distribution," *IEEE Access*, vol. 7, pp. 98182–98196, 2019.
[16] J.-S. Lee, H.-W. Sim, J. Kim, and K.-B. Lee, "Combination analysis and switching method of a cascaded H-bridge multilevel inverter based on transformers with the different turns ratio for increasing the voltage level," *IEEE Trans. Ind. Electron.*, vol. 65, no. 6, pp. 4454–4465, Jun. 2018.
[17] C. Verdugo, J. I. Candela, F. Blaabjerg, and P. Rodriguez, "Three-phase isolated multimodular converter in renewable energy distribution systems," *IEEE J. Emerg. Sel. Topics Power Electron.*, vol. 8, no. 1, pp. 854–865, Mar. 2020.
[18] M. Mazuela, I. Baraia, A. Sanchez-Ruiz, I. Echeverria, I. Torre, and I. Atutxa, "DC-link voltage balancing strategy based on SVM and reactive power exchange for a 5L-MPC back-to-back converter for medium-voltage drives," *IEEE Trans. Ind. Electron.*, vol. 63, no. 12, pp. 7864–7875, Dec. 2016.
[19] H. Tian and Y. W. Li, "An active capacitor voltage balancing method for seven-level hybrid clamped (7L-HC) converter in motor drives," *IEEE Trans. Power Electron.*, vol. 35, no. 3, pp. 2372–2388, Mar. 2020.
[20] S. Rivera, B. Wu, S. Kouro, H. Wang, and D. Zhang, "Cascaded H-bridge multilevel converter topology and three-phase balance control for large scale photovoltaic systems," in *Proc. 3rd IEEE Int. Symp. Power Electron. Distrib. Gener. Syst. (PEDG)*, Aalborg, Denmark, Jun. 2012, pp. 690–697.
[21] Y. Yu, G. Konstantinou, B. Hredzak, and V. G. Agelidis, "Power balance optimization of cascaded H-Bridge multilevel converters for large-scale photovoltaic integration," *IEEE Trans. Power Electron.*, vol. 31, no. 2, pp. 1108–1120, Feb. 2016.
[22] Z. Liu, B. Liu, S. Duan, and Y. Kang, "A novel DC capacitor voltage balance control method for cascade multilevel STATCOM," *IEEE Trans. Power Electron.*, vol. 27, no. 1, pp. 14–27, Jan. 2012.
[23] S. Kouro, B. Wu, A. Moya, E. Villanueva, P. Correa, and J. Rodriguez, "Control of a cascaded H-bridge multilevel converter for grid connection of photovoltaic systems," in *Proc. 35th Annu. Conf. IEEE Ind. Electron.*, Porto, Portugal, Nov. 2009, pp. 3976–3982.
[24] C. Verdugo, S. Kouro, C. A. Rojas, M. A. Perez, T. Meynard, and M. Malinowski, "Five-level T-type cascade converter for rooftop grid-connected photovoltaic systems," *Energies*, vol. 12, no. 9, p. 1743, 2019.

CRISTIAN VERDUGO (Student Member, IEEE) received the B.Sc. and M.Sc. degrees in electronics engineering from Federico Santa Maria Technical University, Valparaiso, Chile, in 2012 and 2014, respectively. He is currently pursuing the Ph.D. degree in electrical engineering with the Research Center of Renewable Electrical Energy Systems, Universitat Politècnica de Catalunya (UPC).

His current research interests include modulation, multilevel converters, photovoltaic power plants, and control of HVDC systems.

JOSE IGNACIO CANDELA (Member, IEEE) received the B.S. and M.S. degrees in industrial engineering and the Ph.D. degree in electrical engineering from the Technical University of Catalonia (UPC), Barcelona, Spain, in 1987, 2000, and 2009, respectively. In 1990, he became an Assistant Professor with UPC, where he later advanced to an Associate Professor, in 1993. He is currently a part of the research group on Renewable Electrical Energy Systems, Department of Electrical Engineering. He has authored or coauthored more than 30 published technical articles and holds several patents. His current research interests include power conditioning, integration of distributed energy systems, and the control of grid-connected power converters. He is also a member of the IEEE Power Electronics Society, the IEEE Industrial Electronics Society, and the IEEE Industry Application Society.

PEDRO RODRIGUEZ (Fellow, IEEE) received the M.Sc. and Ph.D. degrees in electrical engineering from the Technical University of Catalonia (UPC), Barcelona, Spain, in 1989 and 2005, respectively. In 1990, he joined UPC as an Assistant Professor, where he still collaborates with UPC as a part-time Professor and as the Director of the Research Center on Renewable Electrical Energy Systems. In 2005, he was a Visiting Researcher with the Center for Power Electronics Systems, Virginia Polytechnic Institute and State University, Blacksburg, VA, USA. In 2006 and 2007, he was a Postdoctoral Researcher with the Department of Energy Technology, Aalborg University, Aalborg, Denmark, where he was a Co-Supervisor of the Vestas Power Program, from 2007 to 2011. From 2011 to 2017, he was the Director of technology in the area of power systems with Abengoa Research, Seville, Spain. In 2017, he joined Loyola University Andalucía, Seville, as a Full Professor and the Director of LoyolaTech. He is one of the 250 top worldwide highly cited researchers in engineering, in 2017, published by ISI Thomson Reuters. He has coauthored one Wiley-IEEE book, over 100 articles in ISI technical journals, and around 300 papers in conference proceedings. He is the holder of 14 licensed patents. His current research interests include distributed power systems, flexible transmission systems, and power conversion. He is also a member of the Sustainability and Renewable Energy Committee of the IEEE Industry Applications Society and the Renewable Energy Systems Technical Committee of the IEEE Industrial Electronics Society. He is also an Associate Editor of the IEEE TRANSACTIONS ON POWER ELECTRONICS.